Coulomb correlated multi-particle polarons

Petr Klenovský[1, 2, *]

[1] *Department of Condensed Matter Physics, Faculty of Science, Masaryk University, Kotlářská 267/2, 61137 Brno, Czech Republic*
[2] *Czech Metrology Institute, Okružní 31, 63800 Brno, Czech Republic*

(Dated: February 4, 2025)

The electronic and emission properties of correlated multi-particle states are studied theoretically using $\mathbf{k}\cdot\mathbf{p}$ and the configuration interaction methods on a well-known and measured GaAs/AlGaAs quantum dots as a test system. The convergence of the calculated energies and radiative lifetimes of Coulomb correlated exciton, biexciton, positive and negative trions to experimentally observed values is reached when the electron-electron and hole-hole exchange interactions are neglected. That unexpected and striking result uncovers a rich structure of multi-particle states in the studied system, which is further quantitatively compared to published measurements in the literature, obtaining astonishingly good agreement. It is proposed that in real experiments the neglected electron-electron and hole-hole exchange interactions are emitted as acoustic phonons during the radiative recombination of the ground state of complexes, leading to the observation of polaronic multi-particle states. Analysis of their energy spectra provides a direct and measurable insight into the Coulomb correlation, being interesting both on the fundamental level and as possible experimentally tunable property in a wide variety of solid-state systems, in particular associated with quantum computing.

Among the key components in quantum networks [1] quantum-light sources are of dominant importance. As one of those, quantum dots (QDs) have been identified as the best solid-state quantum light emitters [2–5]. Since their discovery [6–9] a considerable improvement was obtained by improving the material quality to reduce charge noise [10, 11], by integrating QDs in photonic structures [3, 12–15], by tailoring the QD properties via external electric [16], magnetic [17], and elastic fields [18–24], and by implementing advanced excitation schemes [14, 25].

Along the experimental development, theoretical computational models were improved as well [26–32], in order to capture the detailed physics of QDs and guide experimental efforts. In principle, such models could be used to design QDs with tailored properties without the need to perform many resource-intensive growth and measurements. If such models are quantitatively validated, they might enable the development of quantum-light sources with increasing complexity.

One of the possibilities to prepare quantum-light photons is the biexciton-exciton cascade [33–38]. Clearly, a model that would correctly predict the energy ordering of the biexciton (XX) with respect to the exciton (X) would be beneficial. It should also find correct energies of negative (X^-) and positive (X^+) trions relative to X as well as the emission rates of all the aforementioned complexes. Clearly, it is crucial to test such a theory with an experimentally reliably measured quantum system. To this end, GaAs QDs in AlGaAs nanoholes [39–47] are chosen in this work. The reason is their high ensemble homogeneity [48–50], negligible built-in strain, and limited intermixing between the GaAs core and AlGaAs barriers.

Although realistic models have been tested in the past, e.g., for GaAs/AlGaAs QDs [38, 40], unfortunately, so far the theory predictions have not reproduced the experimentally observed values, even when realistic QD structural properties or elaborate theory models were used [29]. Here we endeavor to change that.

The multi-particle states in this work are computed using a combination of the eight-band $\mathbf{k}\cdot\mathbf{p}$ method [26, 32, 51, 52], which provides the basis states for the configuration interaction (CI) [31, 53–57] algorithm.

In the calculations of single-particle states first the simulation model structure is defined on rectangular grid. The elastic strain including the effects of nonlinear piezoelectricity [58–60] is then solved in the entire simulation space using the continuum elasticity method [51, 61]. After that, a self-consistent solution of the Poisson and eight-band $\mathbf{k}\cdot\mathbf{p}$ Schrödinger equations is performed. The latter step leads to optimization of the spatial positions and extent of the electron and hole states confined in the structure. As a result of the above calculation, the single-particle eigenenergies $\mathcal{E}_k^{(e)}$ and $\mathcal{E}_l^{(h)}$ of electrons and holes, respectively, as well as the corresponding eigenfunctions $\psi_k^{(e)}$ and $\psi_l^{(h)}$ are obtained, with k and l labeling the states [62].

From the set $\{\psi_k^{(e)}, \psi_l^{(h)}\}$ the Slater determinants (SDs) labeled as $\left|D_m^{\mathrm{M}}\right\rangle$, where $M \in \{\mathrm{X}, \mathrm{X}^-, \mathrm{X}^+, \mathrm{XX}\}$, are assembled. Next, multi-particle states are formed as $\Psi_i^{\mathrm{M}}(\mathbf{r}) = \sum_{m=1}^{n_{\mathrm{SD}}} \eta_{i,m} \left|D_m^{\mathrm{M}}\right\rangle$, where n_{SD} is the number of SDs considered and $\eta_{i,m}$ is the i th CI coefficient that is found along with the CI eigenenergy E_i^{M} using the variational method by solving the Schrödinger equation $\hat{H}^{\mathrm{M}}\Psi_i^{\mathrm{M}}(\mathbf{r}) = E_i^{\mathrm{M}}\Psi_i^{\mathrm{M}}(\mathbf{r})$. The CI Hamiltonian reads $\hat{H}_{mn}^{\mathrm{M}} = \delta_{mn}\left(\mathcal{E}_m^{(e)} - \mathcal{E}_m^{(h)}\right) + \left\langle D_m^{\mathrm{M}}\right| \hat{V}^{\mathrm{M}} \left|D_n^{\mathrm{M}}\right\rangle$, where δ_{mn} is the Kronecker delta and $\left\langle D_m^{\mathrm{M}}\right| \hat{V}^{\mathrm{M}} \left|D_n^{\mathrm{M}}\right\rangle = \mathcal{N}\sum_{ijkl} V_{ij,kl}^{\mathrm{M}}$ for $\{i,j\} \in S_m$ and $\{k,l\} \in S_n$. The sets S_m and S_n

contain indices of single-particle wavefunctions in SDs $\left|D_m^{\mathrm{M}}\right\rangle$ and $\left|D_n^{\mathrm{M}}\right\rangle$, respectively. The normalization factor is $\mathcal{N} = 1/4$ except if $m = n$ and $\{i, j\} = \{k, l\}$ in which case $\mathcal{N} = 1/2$. Furthermore, $V_{ij,kl}^{\mathrm{M}}$ reads

$$V_{ij,kl}^{\mathrm{M}} \equiv (1-\delta_{ij})(1-\delta_{kl})\, q_i q_j \left(J_{ij,kl}^{\mathrm{M}} - K_{ij,lk}^{\mathrm{M}}\right), \qquad (1)$$

where δ_{ij} and δ_{kl} are the Kronecker deltas, thus, the first two brackets ensure that each single-particle state in SDs occurs only once; $q_i, q_j \in \{-1, 1\}$, mark the signs of the charges represented by densities $|\psi_i|^2$ and $|\psi_j|^2$. The parameters $J_{ij,kl}^{\mathrm{M}}$ and $K_{ij,lk}^{\mathrm{M}}$ in Eq. (1) are the direct and the exchange Coulomb integrals between $\langle\psi_i\psi_j|$ and $|\psi_k\psi_l\rangle$. During the CI computation the rate F_{fi}^{M} of the radiative transition between the initial and final CI states, labeled i and f, respectively, is evaluated using the Fermi's golden rule [57, 63–65].

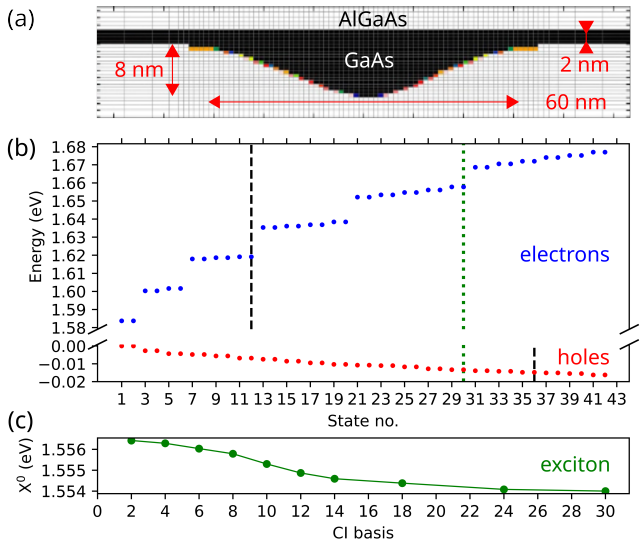

FIG. 1. The simulated structure of GaAs QD with 2 nm GaAs wetting layer (WL) in $Al_{0.4}Ga_{0.6}As$ is shown in panel (a) with marked QD and WL dimensions [52, 66]. Panel (b) gives the single-particle energies of the simulated QD for electrons (blue symbols) and holes (red symbols). For each kind of quasiparticle the energies of 42 states are shown in (b). The doubling of states for each energy level in (b) corresponds to the Pauli doublets of corresponding states. In panel (c) the ground state exciton energy (X^0) is shown as a function of symmetric CI basis size. Note that the change of X^0 energy for the largest bases is less than 50 μeV. For comparison, the measured value was $X^0 = 1.551152$ eV [52]. The black broken and green dotted vertical lines in (b) correspond to the largest CI bases used in this work for computations of $\mathrm{M} \in \{X^-, X^+, XX\}$ and that for X^0, respectively.

As a test structure for the model in this work, we consider realistic GaAs/$Al_{0.4}Ga_{0.6}As$ QD defined using AFM nanohole scan in Fig. 1 (a), being the same as that in Refs. [52, 66]. In Fig. 1 (b) 42 single-particle energies of electrons and holes for QD defined in (a) are given. Clearly, the energies of holes are much more closely spaced than those of electrons [31]. That is a consequence of the different effective masses being $0.067\, m_e$ and $0.51\, m_e$ for electrons and heavy holes in GaAs [67], respectively. Finally, in Fig. 1 (c) the convergence of the energy of the correlated ground state exciton (X^0) with symmetric CI basis (i.e. the same number of $\psi^{(e)}$ and $\psi^{(h)}$) size is shown. The CI convergence to $X^0 = 1.5543$ eV is reached for a CI basis of 30 $\psi^{(e)}$ and 30 $\psi^{(h)}$, at which point the change in X^0 energy with CI basis increase is less than 50 μeV. Regardless of the size of the CI basis, the magnitude of the fine-structure splitting (FSS) of the bright X^0 pair is found as $6 \pm 0.5\,\mu$eV. Note that the experimentally observed values were $X^0 = 1.551152$ eV (8.1 μeV) for exciton energy (FSS) [52], i.e., 3 meV smaller (2 μeV larger) than the converged value from the CI calculations, which is a very good agreement.

In case of complexes consisting of more than one electron or one hole, the key numerical issue in CI implementation is related to the combinatorial complexity of generating all available SDs for a given number of single-particle CI basis states [31, 38]. Since that number is the variational parameter in CI, an increase of that leads to an exponential increase of the number of necessary SDs. To limit that one can, e.g., consider SDs that contain only one or two excited single-particle states, a method called singles-doubles CI (SDCI) [27, 31, 68]. Another possibility of reducing the number of SDs is to consider an asymmetric CI basis, i.e., with different numbers of $\psi^{(e)}$ and $\psi^{(h)}$. That is verified by the fact that the energy densities of $\mathcal{E}^{(e)}$ and $\mathcal{E}^{(h)}$ are markedly different, as seen in Fig. 1 (b). Note that in Fig. 1 (b) all computed $\mathcal{E}^{(e)}$ span 93 meV, while the same number of $\mathcal{E}^{(h)}$ spans only 16 meV.

In Fig. 2 the CI convergence with the number of CI basis states is shown for X^-, X^+, and XX with respect to X^0. Due to the numerical complexity of CI previously discussed, three levels of approximations are used with an increase of CI basis size: (i) symmetric CI basis, i.e., same number of $\psi^{(e)}$ and $\psi^{(h)}$; (ii) the same as for previous point but for SDCI approximation; (iii) SDCI for the asymmetric CI basis composed of twelve $\psi^{(e)}$ and variable number of $\psi^{(h)}$. In all CI and SDCI calculations of complexes in this work, the direct Coulomb integrals (J) between all quasiparticles are considered. However, two scenarios are discussed for the Coulomb exchange interaction (K) as indicated in Fig. 2 (a) and (b). In (a), all Coulomb exchange is considered between all quasiparticles, while in (b) the electron-electron (K_{ee}) and hole-hole (K_{hh}) Coulomb exchange interactions are neglected while the electron-hole (K_{eh}) exchange integrals are preserved.

In agreement with previous reports [31], in Fig. 2 (c) and (d) without correlation X^- is found to be binding while X^+ and XX are anti-binding. An increase in the size of the CI basis and associated

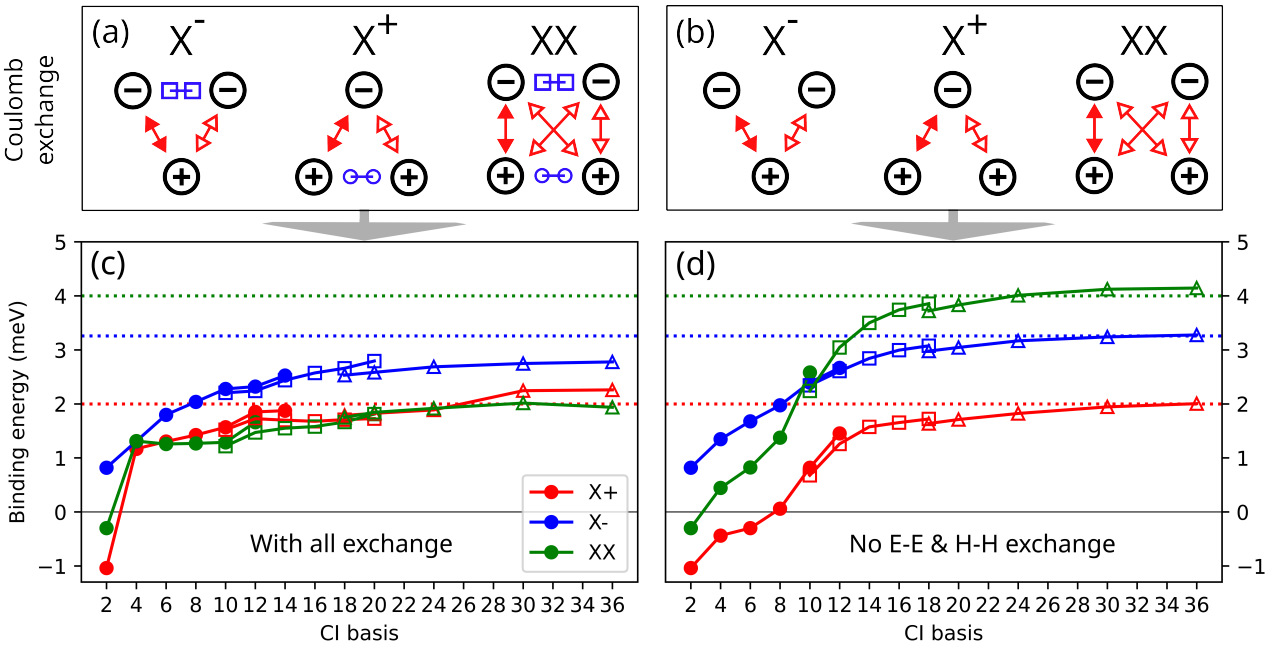

FIG. 2. Panels (a) and (b) show the sketches of the type of the Coulomb exchange considered in CI calculations for X^-, X^+, and XX. The red triangles in (a) and (b) mark the electron-hole exchange interaction (K_{eh}), blue boxes in (a) mark the electron-electron (K_{ee}) and balls hole-hole (K_{hh}) Coulomb exchange. The full symbols in (a) and (b) mark K_{eh} of the final exciton state while empty symbols mark the remaining exchange interaction of the complex after recombination. In (c) and (d) the convergences with respect to the number of single-particle states in CI basis for the binding energies of X^-, X^+, and XX relative to X^0 are shown. In correspondence to (a) and (b), in (c) all Coulomb direct and exchange integrals are considered, while in (d) K_{ee} and K_{hh} are omitted. The meaning of markers in (c) and (d) is the following: (i) full balls represent symmetric CI basis, i.e., same number of $\psi^{(e)}$ and $\psi^{(h)}$; (ii) open squares represent the same but for SDCI approximation; (iii) open upward triangles give SDCI for asymmetric basis composed of twelve $\psi^{(e)}$ and varying number of $\psi^{(h)}$. Note that there is a negligible energy offset $< 100\,\mu$eV between the calculations for the aforementioned CI bases. The red horizontal broken line denotes experimental binding energy of X^+ [52], blue of X^- [69], and green of XX [48]. Notice that calculations converge to experimental values of binding energies in (d), i.e., for calculation with K_{ee} and K_{hh} omitted.

correlation causes X^+ and XX to become binding as well. The convergence of the binding energies of X^-, X^+, and XX is reached (the change in energy is less than 50 μeV) in Fig. 2 (c) and (d) for the SDCI with the basis consisting of 12 $\psi^{(e)}$ and 36 $\psi^{(h)}$ which is called the 12x36 SDCI basis in the following. Although in Fig. 2 (c) X^+ converges towards the experimental value [52], X^- reaches a magnitude somewhat smaller than reported in the measurements [69]. However, the calculations preserve at least the binding energy ordering of X^+ and X^-, i.e. the magnitude of the former being smaller. Sadly, XX misses the experimental target by almost 2 meV. Although similar results were previously observed for smaller GaAs QDs [40], the convergence to experiment is unsatisfactory in Fig. 2 (c).

Surprisingly, the convergence towards the experiment for the 12x36 SDCI basis is considerably improved for all complexes in Fig. 2 (d), where K_{ee} and K_{hh} are neglected [38, 70]. The improvement is particularly striking for XX, the binding energy of which almost doubles between Fig. 2 (c) and (d) reaching very close to the measured value. We note that in all calculations the energy of the correlated electron-hole exchange interaction K_{eh} is 0.01 meV for trions and 0.18 meV for biexciton confirming that correlated direct Coulomb interaction J mainly causes the large binding energy of complexes in Fig. 2 (c) and (d) [31, 38].

The difference between Fig. 2 (c) and (d) is solely in the amount of correlated K_{ee} and K_{hh}, which naturally depend also on the complex M. For notational convenience, we now define for each complex M a variable $M_{eh} = J^M + K^M_{eh}$, where J^M is the total correlated direct and K^M_{eh} the total electron-hole exchange Coulomb interaction between all particles in M. Thus, e.g., biexciton in Fig. 2 (c) is $\mathrm{XX}_{eh} + K^{\mathrm{XX}}_{ee} + K^{\mathrm{XX}}_{hh}$ while that in Fig. 2 (d) is just XX_{eh}. By sequentially neglecting K^{XX}_{ee} and K^{XX}_{hh} in CI calculations one also obtains $\mathrm{XX}_{eh} + K^{\mathrm{XX}}_{hh}$ and $\mathrm{XX}_{eh} + K^{\mathrm{XX}}_{ee}$, or even K^M_{eh} when all exchange interactions are neglected [72].

The results of the aforementioned procedure for the binding energies relative to X^0 and radiative lifetimes calculated by 12x36 SDCI of all complexes studied in this work are summarized in Tab. I. Note that the radiative lifetimes (L) in Tab. I are computed as $L = 1/F^M_{fi}$, where

TABLE I. Computed binding energies (B) relative to exciton and radiative lifetimes (L) of complexes defined in the second column, see also main text. The values of L in the brackets in the fourth column correspond to L corrected by superradiance effect [71], see main text. The complexes are ordered from top to bottom by the magnitude of B.

no.	complex	B (meV)	L (ps)
1	XX_{eh}	4.24	267 (182)
2	X^{-}_{eh}	3.37	192 (131)
3	$\mathrm{XX}_{eh} + K^{\mathrm{XX}}_{ee}$	3.13	228 (155)
4	$\mathrm{X}^{-}_{eh} + K^{\mathrm{X}^-}_{ee}$	2.78	171 (116)
5	$\mathrm{XX}_{eh} + K^{\mathrm{XX}}_{hh}$	2.75	147 (100)
6	$\mathrm{X}^{+}_{eh} + K^{\mathrm{X}^+}_{hh}$	2.34	100 (68)
7	X^{+}_{eh}	2.11	316 (215)
8	$\mathrm{XX}_{eh} + K^{\mathrm{XX}}_{ee} + K^{\mathrm{XX}}_{hh}$	2.02	125 (85)
9	X^0	0	382 (260)

F^M_{fi} is the radiative rate defined previously and given by Fermi's golden rule [54, 63]. Furthermore, in last column of Tab. I in brackets the result of supperradiance [71] correction to L is given. That was calculated as L multiplied by $V_{\mathrm{Bohr}}/V_{\mathrm{QD}} = 0.68$, where V_{QD} is volume of QD and $V_{\mathrm{Bohr}} = 4/3\pi a_0^3$; $a_0 = 11.52$ nm being the Bohr radius in GaAs [57, 73]. The computed L of X^0 and XX_{eh} (lines 9 and 1 in Tab. I) are 382 ps and 267 ps, respectively, i.e. somewhat larger than the reported experimental values of 267 ps and 115 ps [74]. However, the agreement is considerably improved by the superradiance [71] effect to 260 ps and 182 ps for X^0 and XX, respectively.

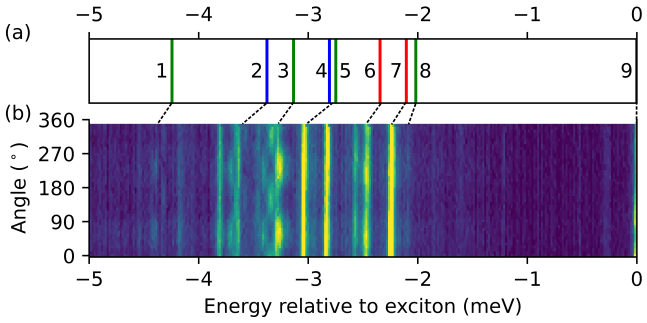

FIG. 3. The vertical lines in (a) show the calculated binding energies of X^+ (red), X^-, (blue), and XX (green) marked by numbers corresponding to the first column of Tab. I. The values are multiplied by -1 to facilitate comparison. Panel (b) shows the polarization resolved micro photoluminescence taken from Ref. [66] for QD1 in absence of applied strain. The broken lines between panels (a) and (b) show the assignment of theory values to experimentally observed bands. Note that both the calculation in (a) and measurement in (b) were performed for temperature of 8 K [52].

To further test the theory results, the calculated binding energies in Tab. I are compared in Fig. 3 to polarization resolved photoluminescence (PL) spectra [52] of QD defined in Fig. 1 (a) and with measured data provided in Ref. [66]. Knowing that the bright band close to −2 meV was previously identified as originating from X^+ [52], the polarization-resolved PL in Fig. 3 (b) enables to assign all the other bands. For instance, XX shows a periodically changing emission intensity with the polarization angle, whereas the intensity of trions does not change with polarization at all. That way, one can, e.g., associate XX_{eh} in Fig. 3 (a) marked by number 1 to a band close to −4.3 meV in Fig. 3 (b). The assignment of all bands is then shown by broken lines between Fig. 3 (a) and (b). Surprisingly, except of a negligible offset of ∼100 μeV, the energies from Tab. I reproduce the PL spectra astonishingly well. We note that the calculated first excited state of XX_{eh} is 3.65 meV above ground state XX_{eh} translating to 0.6 meV binding energy relative to X^0. Since all the other XX-like complexes in Tab. I show similar values of energy difference between ground and first excited state, it rules out the assignment of bands like in Fig. 3 (b) to hot XX states as was assumed elsewhere [38].

TABLE II. Correlated Coulomb exchange interaction energies computed from states in Tab. I. The left column marks the numbers of states which are subtracted from first column of Tab. I. The middle and right column show the assignment of the exchange energy and the magnitude of that, respectively.

subs.	kind	energy (meV)
1-8	$K^{\mathrm{XX}}_{hh} + K^{\mathrm{XX}}_{ee}$	2.22
1-5	K^{XX}_{hh}	1.49
1-3	K^{XX}_{ee}	1.11
2-4	$K^{\mathrm{X}^-}_{ee}$	0.59
6-7	$K^{\mathrm{X}^+}_{hh}$	0.23

It remains to be answered how the energies of the electron-electron and hole-hole Coulomb exchange are dissipated during recombination if for some of the states they are not emitted as photons. A clue about that is provided in Tab. II, where we see that the magnitudes of the exchange energies are close to 1 meV which is a typical energy of the acoustic phonons in the GaAs crystal lattice [75]. Moreover, the electron-phonon interaction is rather strong for longitudinal lattice acoustic phonons [76–78], the interaction times of that being on the order of picoseconds [79–81]. Somewhat similarly to decay of dark excitons [82], since the radiative lifetimes of multi-excitonic complexes are two orders of magnitude longer (see last column in Tab. I) than phononic lifetimes, we anticipate that interaction of QD electronic states with crystal lattice [69] strongly influences the emission of correlated multi-particle complexes providing another dissipative channel and, thus, the complexes behave as a sort of correlated multi-particle polarons [78, 83].

In conclusion, in this work the electronic and emission structure of correlated multi-particle states is studied theoretically using $\mathbf{k}\cdot\mathbf{p}$ and configuration interaction methods. In particular, the convergence of the calculated energies and radiative lifetimes of Coulomb corre-

lated X, X^-, X^+, and XX to experimentally observed values is achieved for a realistic GaAs/AlGaAs quantum dot structure, chosen as a test system. It is identified that an interaction of the multi-particle states with the crystal lattice provides a dissipation mechanism for the emission of the exchange interaction energy between particles with the same charge within the multi-particle complex. That enables the observation of polaronic multi-particle states, providing a direct way of measuring the correlated exchange interaction between various quasi-particles, and procure possibilities of tuning that by various methods that are already experimentally available such as externally applied electric [16], magnetic [17], or elastic fields [18–22]. Furthermore, external tuning of electron-electron and hole-hole exchange interaction might provide a tool for the development and operation of structures for quantum computation [84, 85]. The results presented here are relevant not only to quantum dots but to virtually any multi-particle system interacting with a bath which enables dissipation of electronic states other than by photons only. That includes a wide variety of solid-state systems as well as enabling experimental studies of the fundamental nature of the exchange interaction in correlated systems.

The author thanks G. Undeutsch, E.A. Chekhovich, X. Yuan, A. Rastelli for fruitful discussions and providing the experimental data. The author acknowledges funding from the European Innovation Council Pathfinder program under grant agreement No 101185617 (QCEED), support by the project Quantum materials for applications in sustainable technologies, CZ.02.01.01/00/22 008/0004572, and partly funding by Institutional Subsidy for Long-Term Conceptual Development of a Research Organization granted to the Czech Metrology Institute by the Ministry of Industry and Trade of the Czech Republic.

* klenovsky@physics.muni.cz

[1] H. J. Kimble, Nature **453**, 1023 (2008).
[2] I. Aharonovich, D. Englund, and M. Toth, Nature Photonics **10**, 631 (2016).
[3] P. Senellart, G. Solomon, and A. White, Nature nanotechnology **12**, 1026 (2017).
[4] X. Zhou, L. Zhai, and J. Liu, Photonics Insights **1**, R07 (2023).
[5] A. M. Fox, Advanced Quantum Technologies , 2300390 (2024).
[6] A. I. Ekimov and A. A. Onushchenko, JETP Letters **118**, S15 (2023).
[7] A. I. Ekimov, A. L. Efros, and A. A. Onushchenko, Solid State Communications **56**, 921 (1985).
[8] D. Leonard, M. Krishnamurthy, C. M. Reaves, S. P. Denbaars, and P. M. Petroff, Applied Physics Letters **63**, 3203 (1993).
[9] K. D. Wegner and U. Resch-Genger, Analytical and Bioanalytical Chemistry **416**, 3283–3293 (2024).
[10] A. V. Kuhlmann, J. H. Prechtel, J. Houel, A. Ludwig, D. Reuter, A. D. Wieck, and R. J. Warburton, Nature Communications **6**, 8204 (2015).
[11] P. Lodahl, A. Ludwig, and R. J. Warburton, Physics Today **75**, 44 (2022).
[12] P. Lodahl, S. Mahmoodian, and S. Stobbe, Reviews of Modern Physics **87**, 347 (2015).
[13] J. Liu, R. Su, Y. Wei, B. Yao, S. F. C. da Silva, Y. Yu, J. Iles-Smith, K. Srinivasan, A. Rastelli, J. Li, and X. Wang, Nature Nanotechnology **14**, 586 (2019).
[14] H. Wang, Y.-M. He, T.-H. Chung, H. Hu, Y. Yu, S. Chen, X. Ding, M.-C. Chen, J. Qin, X. Yang, R.-Z. Liu, Z.-C. Duan, J.-P. Li, S. Gerhardt, K. Winkler, J. Jurkat, L.-J. Wang, N. Gregersen, Y.-H. Huo, Q. Dai, S. Yu, S. Höfling, C.-Y. Lu, and J.-W. Pan, Nature Photonics **13**, 770 (2019).
[15] N. Tomm, A. Javadi, N. O. Antoniadis, D. Najer, M. C. Löbl, A. R. Korsch, R. Schott, S. R. Valentin, A. D. Wieck, A. Ludwig, and R. J. Warburton, Nature Nanotechnology **16**, 399 (2021).
[16] A. J. Bennett, M. A. Pooley, R. M. Stevenson, M. B. Ward, R. B. Patel, A. B. De La Giroday, N. Sköd, I. Farrer, C. A. Nicoll, D. A. Ritchie, and A. J. Shields, Nature Physics **6**, 947 (2010).
[17] M. Bayer, G. Ortner, O. Stern, A. Kuther, A. A. Gorbunov, A. Forchel, P. Hawrylak, S. Fafard, K. Hinzer, T. L. Reinecke, S. N. Walck, J. P. Reithmaier, F. Klopf, and F. Schäfer, Physical Review B - Condensed Matter and Materials Physics **65**, 1953151 (2002).
[18] H. O. Oyoko, C. A. Duque, and N. Porras-Montenegro, Journal of Applied Physics **90** (2001).
[19] S. Seidl, M. Kroner, A. Högele, K. Karrai, R. J. Warburton, A. Badolato, and P. M. Petroff, Applied Physics Letters **88**, 203113 (2006).
[20] R. Singh and G. Bester, Physical Review Letters **104**, 196803 (2010).
[21] M. Gong, W. Zhang, G. C. Guo, and L. He, Physical Review Letters **106**, 227401 (2011).
[22] J. Martín-Sánchez, R. Trotta, A. Mariscal, R. Serna, G. Piredda, S. Stroj, J. Edlinger, C. Schimpf, J. Aberl, T. Lettner, J. Wildmann, H. Huang, X. Yuan, D. Ziss, J. Stangl, and A. Rastelli, Semiconductor Science and Technology **33**, 013001 (2018).
[23] I. Limame, C. W. Shih, A. Koltchanov, F. Heisinger, F. Nippert, M. Plattner, J. Schall, M. R. Wagner, S. Rodt, P. Klenovsky, and S. Reitzenstein, Applied Physics Letters **124**, 61102 (2024).
[24] C.-W. Shih, I. Limame, C. C. Palekar, A. Koulas-Simos, A. Kaganskiy, P. Klenovský, and S. Reitzenstein, Laser & Photonics Reviews **18**, 2301242 (2024).
[25] F. Sbresny, L. Hanschke, E. Schöll, W. Rauhaus, B. Scaparra, K. Boos, E. Zubizarreta Casalengua, H. Riedl, E. del Valle, J. J. Finley, K. D. Jöns, and K. Müller, Physical Review Letters **128**, 093603 (2022).
[26] O. Stier, Ph.D. thesis, Technische Universität Berlin, (2000).
[27] M. Braskén, M. Lindberg, D. Sundholm, and J. Olsen, Physical Review B **61**, 7652 (2000).
[28] N. Baer, S. Schulz, S. Schumacher, P. Gartner, G. Czycholl, and F. Jahnke, Applied Physics Letters **87**, 231114 (2005).
[29] G. Bester, A. Zunger, X. Wu, and D. Vanderbilt, Physical Review B - Condensed Matter and Materials Physics

74, 081305(R) (2006).
[30] S. Tomić and N. Vukmirović, Physical Review B **79**, 245330 (2009).
[31] A. Schliwa, M. Winkelnkemper, and D. Bimberg, Physical Review B **79**, 075443 (2009).
[32] A. Mittelstädt, A. Schliwa, and P. Klenovský, Light: Science & Applications **11**, 17 (2022).
[33] R. Winik, D. Cogan, Y. Don, I. Schwartz, L. Gantz, E. R. Schmidgall, N. Livneh, R. Rapaport, E. Buks, and D. Gershoni, Physical Review B **95** (2017).
[34] J. Kettler, M. Paul, F. Olbrich, K. Zeuner, M. Jetter, P. Michler, M. Florian, C. Carmesin, and F. Jahnke, Physical Review B **94** (2016).
[35] Y. M. He, O. Iff, N. Lundt, V. Baumann, M. Davanco, K. Srinivasan, S. Höfling, and C. Schneider, Nature Communications 2016 7:1 **7**, 1 (2016).
[36] I. Ozfidan, M. Korkusinski, and P. Hawrylak, Physical Review B - Condensed Matter and Materials Physics **91** (2015).
[37] D. Huber, M. Reindl, J. Aberl, A. Rastelli, and R. Trotta, Journal of Optics **20**, 073002 (2018).
[38] B. U. Lehner, T. Seidelmann, G. Undeutsch, C. Schimpf, S. Manna, M. Gawełczyk, S. F. C. da Silva, X. Yuan, S. Stroj, D. E. Reiter, V. M. Axt, and A. Rastelli, Nano Letters **23**, 1409 (2023).
[39] A. Rastelli, S. Stufler, A. Schliwa, R. Songmuang, C. Manzano, G. Costantini, K. Kern, A. Zrenner, D. Bimberg, and O. G. Schmidt, Physical Review Letters **92**, 166104 (2004).
[40] L. Wang, V. Křápek, F. Ding, F. Horton, A. Schliwa, D. Bimberg, A. Rastelli, and O. G. Schmidt, Physical Review B - Condensed Matter and Materials Physics **80**, 085309 (2009).
[41] J. D. Plumhof, V. Křápek, L. Wang, A. Schliwa, D. Bimberg, A. Rastelli, and O. G. Schmidt, Physical Review B - Condensed Matter and Materials Physics **81**, 121309 (2010).
[42] J. D. Plumhof, R. Trotta, V. Křápek, E. Zallo, P. Atkinson, S. Kumar, A. Rastelli, and O. G. Schmidt, Physical Review B **87**, 075311 (2013).
[43] Y. H. Huo, B. J. Witek, S. Kumar, J. R. Cardenas, J. X. Zhang, N. Akopian, R. Singh, E. Zallo, R. Grifone, D. Kriegner, R. Trotta, F. Ding, J. Stangl, V. Zwiller, G. Bester, A. Rastelli, and O. G. Schmidt, Nature Physics **10**, 46 (2013).
[44] X. Yuan, F. Weyhausen-Brinkmann, J. Martín-Sánchez, G. Piredda, V. Křápek, Y. Huo, H. Huang, C. Schimpf, O. G. Schmidt, J. Edlinger, G. Bester, R. Trotta, and A. Rastelli, Nature Communications **9**, 3058 (2018).
[45] H. Huang, D. Csontosová, S. Manna, Y. Huo, R. Trotta, A. Rastelli, and P. Klenovský, Physical Review B **104**, 165401 (2021).
[46] C. Heyn, M. Klingbeil, C. Strelow, A. Stemmann, S. Mendach, and W. Hansen, Nanoscale Research Letters **5**, 1633 (2010).
[47] M. C. Löbl, L. Zhai, J.-P. Jahn, J. Ritzmann, Y. Huo, A. D. Wieck, O. G. Schmidt, A. Ludwig, A. Rastelli, and R. J. Warburton, Physical Review B **100**, 155402 (2019).
[48] S. F. C. da Silva, G. Undeutsch, B. Lehner, S. Manna, T. M. Krieger, M. Reindl, C. Schimpf, R. Trotta, and A. Rastelli, Applied Physics Letters **119**, 120502 (2021).
[49] R. Keil, M. Zopf, Y. Chen, B. Höfer, J. Zhang, F. Ding, and O. G. Schmidt, Nature Communications **8** (2017).
[50] A. Rastelli, R. Songmuang, and O. G. Schmidt, Physica E: Low-Dimensional Systems and Nanostructures **23**, 384 (2004).
[51] S. Birner, T. Zibold, T. Andlauer, T. Kubis, M. Sabathil, A. Trellakis, and P. Vogl, IEEE Transactions on Electron Devices **54**, 2137 (2007).
[52] X. Yuan, S. F. C. D. Silva, D. Csontosová, H. Huang, C. Schimpf, M. Reindl, J. Lu, Z. Ni, A. Rastelli, and P. Klenovský, Physical Review B **107**, 235412 (2023).
[53] M. C. Troparevsky and A. Franceschetti, Journal of Physics: Condensed Matter **20**, 055211 (2008).
[54] P. Klenovský, P. Steindl, and D. Geffroy, Scientific Reports **7**, 45568 (2017).
[55] P. Klenovský, A. Schliwa, and D. Bimberg, Physical Review B **100**, 115424 (2019).
[56] D. Csontosová and P. Klenovský, Physical Review B **102**, 125412 (2020).
[57] "See supplemental material at [url will be inserted by publisher] for further details about the theory used in this work." ().
[58] G. Bester, X. Wu, D. Vanderbilt, and A. Zunger, Physical Review Letters **96**, 187602 (2006).
[59] A. Beya-Wakata, P. Y. Prodhomme, and G. Bester, Physical Review B **84**, 195207 (2011).
[60] P. Klenovský, P. Steindl, J. Aberl, E. Zallo, R. Trotta, A. Rastelli, and T. Fromherz, Physical Review B **97**, 245314 (2018).
[61] T. Zibold, Ph.D. thesis, Technische Universität München, (2007).
[62] "See supplemental material at [url will be inserted by publisher] for influence of k.p solver settings on presented results." ().
[63] P. Dirac, Proceedings of the Royal Society of London. Series A, Containing Papers of a Mathematical and Physical Character **114**, 243 (1927).
[64] M. Zielinski, M. Korkusinski, and P. Hawrylak, Physical Review B **81**, 085301 (2010).
[65] P. Klenovský, D. Hemzal, P. Steindl, M. Zíková, V. Křápek, and J. Humlíček, Physical Review B **92**, 241302 (2015).
[66] X. Yuan, P. Klenovsky, and A. Rastelli, (2023).
[67] I. Vurgaftman, J. R. Meyer, and L. R. Ram-Mohan, Journal of Applied Physics **89**, 5815 (2001).
[68] C. D. Sherrill and H. F. Schaefer, Advances in Quantum Chemistry **34**, 143 (1999).
[69] D. Huber, B. U. Lehner, D. Csontosová, M. Reindl, S. Schuler, S. F. Covre da Silva, P. Klenovský, and A. Rastelli, Physical Review B **100**, 235425 (2019).
[70] G. Hönig, G. Callsen, A. Schliwa, S. Kalinowski, C. Kindel, S. Kako, Y. Arakawa, D. Bimberg, and A. Hoffmann, Nature Communications **5**, 5721 (2014).
[71] P. Tighineanu, R. S. Daveau, T. B. Lehmann, H. E. Beere, D. A. Ritchie, P. Lodahl, and S. Stobbe, Physical Review Letters **116** (2016).
[72] "See supplemental material at [url will be inserted by publisher] for influence of electron-hole exchange interaction on calculations of multi-particle states." ().
[73] S. Stobbe, T. W. Schlereth, S. Höfling, A. Forchel, J. M. Hvam, and P. Lodahl, Physical Review B - Condensed Matter and Materials Physics **82** (2010).
[74] C. Schimpf, M. Reindl, P. Klenovský, T. Fromherz, S. F. Covre da Silva, J. Hofer, C. Schneider, S. Höfling, R. Trotta, and A. Rastelli, Optics Express **27**, 35290 (2019).
[75] P. Y. Yu and M. Cardona, *Fundamentals of semiconduc-*

tors : physics and materials properties (Springer, 2010) p. 775.
[76] B. Krummheuer, V. M. Axt, and T. Kuhn, Physical Review B **65**, 1 (2002).
[77] D. E. Reiter, T. Kuhn, M. Glässl, and V. M. Axt, Journal of Physics: Condensed Matter **26**, 423203 (2014).
[78] J. Iles-Smith, D. P. McCutcheon, A. Nazir, and J. Mørk, Nature Photonics 2017 11:8 **11**, 521 (2017).
[79] J. C. Mattos, W. O. Guimarães, and R. C. Leite, Optics Communications **8**, 73 (1973).
[80] A. A. Maznev, F. Hofmann, A. Jandl, K. Esfarjani, M. T. Bulsara, E. A. Fitzgerald, G. Chen, and K. A. Nelson, Applied Physics Letters **102** (2013).
[81] Y. Choi, S. Sim, S. C. Lim, Y. H. Lee, and H. Choi, Scientific Reports 2013 3:1 **3**, 1 (2013).
[82] K. Roszak, V. M. Axt, T. Kuhn, and P. Machnikowski, Physical Review B - Condensed Matter and Materials Physics **76** (2007).
[83] J. Iles-Smith and A. Nazir, Optica, Vol. 3, Issue 2, pp. 207-211 **3**, 207 (2016).
[84] D. Loss and D. P. DiVincenzo, Physical Review A **57**, 120 (1998).
[85] S. E. Economou, N. Lindner, and T. Rudolph, Physical Review Letters **105** (2010).

Supplementary information for the manuscript: Coulomb correlated multi-particle polarons

Petr Klenovský[1, 2, a)]
[1)] *Department of Condensed Matter Physics, Faculty of Science, Masaryk University, Kotlářská 267/2, 61137 Brno, Czech Republic*
[2)] *Czech Metrology Institute, Okružní 31, 63800 Brno, Czech Republic*

SI. SINGLE-PARTICLE STATES

In the calculations, we first implement the 3D QD model structure (size, shape, chemical composition). This is followed by the calculation of elastic strain by minimizing the total strain energy in the structure and subsequent evaluation of piezoelectricity up to non-linear terms.[1–3] The resulting strain and polarization fields then enter the eight-band $\mathbf{k}\cdot\mathbf{p}$ Hamiltonian.

In $\mathbf{k}\cdot\mathbf{p}$, we consider the single-particle states as linear combinations of s-orbital like and x, y, z p-orbital like Bloch waves[4,5] at Γ point of the Brillouin zone, i.e.,

$$\psi_{a_n}(\mathbf{r}) = \sum_{\nu\in\{s,x,y,z\}\otimes\{\uparrow,\downarrow\}} \chi_{a_n,\nu}(\mathbf{r}) u^{\Gamma}_{\nu}, \tag{1}$$

where u^{Γ}_{ν} is the Bloch wavefunction of s- and p-like conduction and valence bands at Γ point, respectively, $\uparrow/\downarrow$ marks the spin, and $\chi_{a_n,\nu}$ is the envelope function for $a_n \in \{e_n, h_n\}$ [e (h) refers to electron (hole)] of the n-th single-particle state. Thereafter, the following envelope-function $\mathbf{k}\cdot\mathbf{p}$ Schrödinger equation is solved

$$\sum_{\nu\in\{s,x,y,z\}\otimes\{\uparrow,\downarrow\}} \left(\left[E^{\Gamma}_{\nu} - \frac{\hbar^2\nabla^2}{2m_e} + V_0(\mathbf{r}) \right] \delta_{\nu'\nu} + \frac{\hbar\nabla\cdot\mathbf{p}_{\nu'\nu}}{m_e} + \hat{H}^{\mathrm{str}}_{\nu'\nu}(\mathbf{r}) + \hat{H}^{\mathrm{so}}_{\nu'\nu}(\mathbf{r}) \right) \chi_{a_n,\nu'}(\mathbf{r}) = \mathscr{E}^{k\cdot p}_n \cdot \chi_{a_n,\nu'}(\mathbf{r}), \tag{2}$$

where the term in round brackets on the left side of the equation is the envelope function $\mathbf{k}\cdot\mathbf{p}$ Hamiltonian $\hat{H}^{k\cdot p}_0$, and $\mathscr{E}^{k\cdot p}_n$ on the right side is the n-th single-particle eigenenergy. Furthermore, E^{Γ}_{ν} is the energy of bulk Γ-point Bloch band ν, $V_0(\mathbf{r})$ is the scalar potential (e.g. due to piezoelectricity), $\hat{H}^{\mathrm{str}}_{\nu'\nu}(\mathbf{r})$ is the Pikus-Bir Hamiltoninan introducing the effect of elastic strain,[5,6] and $\hat{H}^{\mathrm{so}}_{\nu'\nu}(\mathbf{r})$ is the spin-orbit Hamiltonian.[6]Further, $\hbar$ is the reduced Planck's constant, m_e the free electron mass, δ the Kronecker delta, and $\nabla := \left(\frac{\partial}{\partial x}, \frac{\partial}{\partial y}, \frac{\partial}{\partial z}\right)^T$.

The aforementioned Schrödinger equation is then solved self-consistently with the Poisson equation to improve the spatial position of electron and hole wavefunctions.[5] Note that the Poisson equation solver used in the single-particle calculations does not include Coulomb exchange.

SII. CONFIGURATION INTERACTION

The single-particle states computed by the aforementioned $\mathbf{k}\cdot\mathbf{p}$ are used as basis states for CI. In CI we consider the multi-particle (M) states as linear combinations of the Slater determinants (SDs). In all generality, for any total number of fermions N in the system, the m-th SD is written as:

$$\left|D^M_m\right\rangle = \frac{1}{\sqrt{N!}} \sum_P (-1)^P \psi_{P(i_1)}(\mathbf{r}_1)\psi_{P(i_2)}(\mathbf{r}_2)\ldots\psi_{P(i_N)}(\mathbf{r}_N), \tag{3}$$

where $N \equiv N_e + N_h$, with N_e (N_h) the number of electrons (holes) in the complex M (e.g., $N_e = 2$, $N_h = 1$ for the negative trion X^-). Moreover, P marks the permutation of wavefunction indices. SDs of the multi-particle states considered in this work are for the neutral exciton X

$$|\mathrm{X}\rangle = \sum_{i=1}^{n_e}\sum_{j=1}^{n_h} \eta^{\mathrm{X}}_{ij} \begin{vmatrix} \psi_{ei}(\mathbf{r}_e) & \psi_{ei}(\mathbf{r}_h) \\ \psi_{hj}(\mathbf{r}_e) & \psi_{hj}(\mathbf{r}_h) \end{vmatrix}, \tag{4}$$

[a)] Electronic mail: klenovsky@physics.muni.cz

for positive trion X^+

$$\left|X^+\right\rangle = \sum_{i=1}^{n_e} \sum_{\substack{j,k=1 \\ k>j}}^{n_h} \eta_{ijk}^{X^+} \begin{vmatrix} \psi_{ei}(\mathbf{r}_e) & \psi_{hj}(\mathbf{r}_e) & \psi_{hk}(\mathbf{r}_e) \\ \psi_{ei}(\mathbf{r}_{h1}) & \psi_{hj}(\mathbf{r}_{h1}) & \psi_{hk}(\mathbf{r}_{h1}) \\ \psi_{ei}(\mathbf{r}_{h2}) & \psi_{hj}(\mathbf{r}_{h2}) & \psi_{hk}(\mathbf{r}_{h2}) \end{vmatrix}, \tag{5}$$

for negative trion X^-

$$\left|X^-\right\rangle = \sum_{\substack{i,j=1 \\ j>i}}^{n_e} \sum_{k=1}^{n_h} \eta_{ijk}^{X^-} \begin{vmatrix} \psi_{ei}(\mathbf{r}_{e1}) & \psi_{ej}(\mathbf{r}_{e1}) & \psi_{hk}(\mathbf{r}_{e1}) \\ \psi_{ei}(\mathbf{r}_{e2}) & \psi_{ej}(\mathbf{r}_{e2}) & \psi_{hk}(\mathbf{r}_{e2}) \\ \psi_{ei}(\mathbf{r}_h) & \psi_{ej}(\mathbf{r}_h) & \psi_{hk}(\mathbf{r}_h) \end{vmatrix}, \tag{6}$$

and for the neutral biexciton XX

$$|XX\rangle = \sum_{\substack{i,j=1 \\ j>i}}^{n_e} \sum_{\substack{k,l=1 \\ k>l}}^{n_h} \eta_{ijkl}^{XX} \begin{vmatrix} \psi_{ei}(\mathbf{r}_{e1}) & \psi_{ej}(\mathbf{r}_{e1}) & \psi_{hk}(\mathbf{r}_{e1}) & \psi_{hl}(\mathbf{r}_{e1}) \\ \psi_{ei}(\mathbf{r}_{e2}) & \psi_{ej}(\mathbf{r}_{e2}) & \psi_{hk}(\mathbf{r}_{e2}) & \psi_{hl}(\mathbf{r}_{e2}) \\ \psi_{ei}(\mathbf{r}_{h1}) & \psi_{ej}(\mathbf{r}_{h1}) & \psi_{hk}(\mathbf{r}_{h1}) & \psi_{hl}(\mathbf{r}_{h1}) \\ \psi_{ei}(\mathbf{r}_{h2}) & \psi_{ej}(\mathbf{r}_{h2}) & \psi_{hk}(\mathbf{r}_{h2}) & \psi_{hl}(\mathbf{r}_{h2}) \end{vmatrix}, \tag{7}$$

where n_e and n_h mark the number of single-particle states for electrons and holes, respectively. Furthermore, the aforementioned SDs defined in the Eqs. (4-7) must be normalized, i.e. $\sum_m |\eta_m|^2 = 1$.

Using the aforementioned $\left|D_m^{\mathrm{M}}\right\rangle$ the multi-particle trial wavefunction reads

$$\Psi_i^{\mathrm{M}}(\mathbf{r}) = \sum_{m=1}^{n_{\mathrm{SD}}} \eta_{i,m} \left|D_m^{\mathrm{M}}\right\rangle, \tag{8}$$

where n_{SD} is the number of Slater determinants $\left|D_m^{\mathrm{M}}\right\rangle$, and $\eta_{i,m}$ is the i-th CI coefficient which is found along with the eigenenergy using the variational method by solving the Schrödinger equation

$$\hat{H}^{\mathrm{M}}\Psi_i^{\mathrm{M}}(\mathbf{r}) = E_i^{\mathrm{M}}\Psi_i^{\mathrm{M}}(\mathbf{r}), \tag{9}$$

where E_i^{M} is the i-th eigenenergy of the multi-particle state $\Psi_i^{\mathrm{M}}(\mathbf{r})$, and $\hat{H}^{\mathrm{M}}$ is the CI Hamiltonian which reads

$$\hat{H}_{mn}^{\mathrm{M}} = \delta_{mn}\left(\mathscr{E}_m^{(e)} - \mathscr{E}_m^{(h)}\right) + \left\langle D_m^{\mathrm{M}}\right| \hat{V}^{\mathrm{M}} \left|D_n^{\mathrm{M}}\right\rangle, \tag{10}$$

where δ_{mn} is the Kronecker delta and $\left\langle D_m^{\mathrm{M}}\right| \hat{V}^{\mathrm{M}} \left|D_n^{\mathrm{M}}\right\rangle = \mathscr{N} \sum_{ijkl} V_{ij,kl}^{\mathrm{M}}$ for $i,j \in S_m$ and $k,l \in S_n$. The sets S_m and S_n contain indices of all single-particle wavefunctions in SDs $\left\langle D_m^{\mathrm{M}}\right|$ and $\left|D_n^{\mathrm{M}}\right\rangle$, respectively. The parameter $\mathscr{N}$ is the normalization factor, see in the following. Furthermore, $V_{ij,kl}^{\mathrm{M}}$ is defined by

$$\begin{aligned} V_{ij,kl}^{\mathrm{M}} &\equiv (1-\delta_{ij})(1-\delta_{kl})\, q_i q_j \frac{e^2}{4\pi\epsilon_0} \iint \left(\frac{\mathrm{d}\mathbf{r}_1 \mathrm{d}\mathbf{r}_2}{\epsilon_r(\mathbf{r}_1,\mathbf{r}_2)|\mathbf{r}_1-\mathbf{r}_2|}\right) \{\psi_i^*(\mathbf{r}_1)\psi_j^*(\mathbf{r}_2)\psi_k(\mathbf{r}_1)\psi_l(\mathbf{r}_2) - \psi_i^*(\mathbf{r}_1)\psi_j^*(\mathbf{r}_2)\psi_l(\mathbf{r}_1)\psi_k(\mathbf{r}_2)\} \\ &= (1-\delta_{ij})(1-\delta_{kl})\, q_i q_j \left(J_{ij,kl}^{\mathrm{M}} - K_{ij,lk}^{\mathrm{M}}\right), \end{aligned} \tag{11}$$

where ϵ_0 and $\epsilon_r(\mathbf{r}_1,\mathbf{r}_2)$ are the vacuum and spatially dependent relative permittivity, respectively, and δ_{ij} and δ_{kl} are the Kronecker deltas. Note that the terms in the first two brackets in Eq. (11) ensure that each single-particle state in SD occurs only once, thus preventing double counting. Furthermore, $q_i, q_j \in \{-1, 1\}$ marks the sign of the charge of the quasiparticles in states with indices i and j, respectively; e is the elementary charge. The parameters J^{M} and K^{M} in Eq. (11) are direct and exchange Coulomb integrals.

Now, since the single-particle states are orthonormal, one finds that in Eq. (10) there are only three possible kinds of matrix elements in CI, i.e.

$$\begin{aligned} \hat{H}_{nm}^{M} &\equiv \left\langle D_m^M\right| \hat{H}^M \left|D_n^M\right\rangle \\ &= \begin{cases} \mathscr{E}_m^{(e)} - \mathscr{E}_m^{(h)} + \dfrac{1}{2} \displaystyle\sum_{i,j\in S_n} & \left(J_{ij,ij}^{\mathrm{M}} - K_{ij,ji}^{\mathrm{M}}\right) \text{ if } m = n \\ \dfrac{1}{4} \displaystyle\sum_{j\in S_n} \left(J_{ij,kj}^{\mathrm{M}} - K_{ij,jk}^{\mathrm{M}}\right) & \text{if } D_m^M \text{ and } D_n^M \text{ differ by one single-particle state: } \left|D_m^M\right\rangle \propto c_i^\dagger c_k \left|D_n^M\right\rangle \\ \dfrac{1}{4}\left(J_{ij,kl}^{\mathrm{M}} - K_{ij,lk}^{\mathrm{M}}\right) & \text{if } D_m^M \text{ and } D_n^M \text{ differ by two single-particle states: } \left|D_m^M\right\rangle \propto c_i^\dagger c_j^\dagger c_k c_l \left|D_n^M\right\rangle,\ k<l. \end{cases} \end{aligned} \tag{12}$$

where the factors before the sums in above equation corresponds to $\mathscr{N}$, mentioned in the main paper. Note that the above matrix elements correspond to a diagonal and one of the triangles of the CI matrix. The other triangular matrix is a complex conjugate of the above offdiagonal elements.

SIII. METHOD OF CALCULATION OF CONFIGURATION INTERACTION

The sixfold integral in Eq. (11) is evaluated using the Green's function method.[4,7] The integral in Eq. (11) is split into solution of the Poisson's equation for one quasiparticle a only, followed by a three-fold integral for quasiparticle b in the electrostatic potential generated by particle a and resulting from the previous step. That procedure, thus, makes the whole solution numerically more feasible and is described by

$$\begin{aligned} \nabla\left[\epsilon(\mathbf{r}_1)\nabla\hat{U}_{ajl}(\mathbf{r}_1)\right] &= \frac{4\pi e^2}{\epsilon_0}\Psi^*_{aj}(\mathbf{r}_1)\Psi_{al}(\mathbf{r}_1), \\ V^M_{ij,kl} &= \int \mathrm{d}\mathbf{r}_2\, \hat{U}_{ajl}(\mathbf{r}_2)\Psi^*_{bi}(\mathbf{r}_2)\Psi_{bk}(\mathbf{r}_2), \end{aligned} \tag{13}$$

where $a, b \in \{e, h\}$.

SIV. RADIATIVE RATE

During computation of CI, the oscillator strength of the optical transition F^{M}_{fi} between the i-th and f-th eigenstate of the excitonic complex, respectively, is evaluated using the Fermi's golden rule[8–10]

$$F^{\mathrm{M}}_{fi} = \left|\left\langle \mathrm{M}_f \left| \hat{P} \right| \mathrm{M}_i \right\rangle\right|^2, \tag{14}$$

where $|\mathrm{M}_f\rangle$ is the final state after recombination of electron-hole pair in $|\mathrm{M}_i\rangle$. The operator $\hat{P}$ is defined by

$$\hat{P} = \sum_{rp} \left\langle \psi_{e_r} \left| \mathbf{e}\cdot\hat{\mathbf{p}} \right| \psi_{h_p} \right\rangle. \tag{15}$$

Here ψ_e and ψ_h are the single-particle wavefunctions for electrons and holes, respectively, $\mathbf{e}$ is the polarization vector and $\hat{\mathbf{p}}$ is the momentum operator. Note that the values of radiative lifetime discussed in the main paper are obtained as an inverse of the rate in Eq (14), i.e. $1/F^{\mathrm{M}}_{fi}$.

The GaAs QDs are known to show the enhancement of radiative emission due to the weak confinement effect.[11] Thus, it is necessary to include this effect in calculations in order to match experimental results. The theory of emission enhancement, dubbed superradiance, was worked out in Ref.[12–14] and results of that are utilized here. Following Ref.[12,13] it turns out that the emission enhancement, e.g., for excitons is due to the wavefunction spread of that being larger than the effective Bohr radius in GaAs. The formula for the latter reads[13]

$$a_0 = \frac{4\pi\hbar^2\epsilon_0\epsilon_r}{e^2 m_0 m_r}, \tag{16}$$

where $\epsilon_r = 12.9$ is the relative permittivity for GaAs[15] and

$$m_r = \frac{m_e m_{hh}}{m_e + m_{hh}}, \tag{17}$$

with $m_e = 0.067$ and $m_{hh} = 0.51$ being the effective masses of electrons and heavy holes, respectively.[15] Plugging all constants into Eq. (16) provides a value of the effective Bohr radius in GaAs $a_0 = 11.52$ nm mentioned in the main paper.

Since GaAs QDs studied as the test system in this work are almost rotationally symmetric for rotations around vertical QD axis,[16] for convenience, one can approximate QD in Fig. 1 (a) of the main paper by a cone with height of $h = 10$ nm and base radius $r = 30$ nm, thus having a volume $V_{\mathrm{QD}} = \frac{1}{3}\pi h r^2$. Assuming now that exciton wavefunction occupies the whole QD volume[17] and spherical volume of exciton in bulk GaAs is $V_{\mathrm{Bohr}} = \frac{4}{3}\pi a_0^3$ one obtains that the radiative rate is enhanced by a superradiance factor f_{sr}

$$f_{\mathrm{sr}} = \frac{V_{\mathrm{QD}}}{V_{\mathrm{Bohr}}} = \frac{1}{4}\frac{h r^2}{a_0^3} = 1.47, \tag{18}$$

accelerating the emission rate from studied GaAs QD. An inverse of Eq. (18) reads $1/f_{\mathrm{sr}} = 0.68$ and reduces the radiative lifetime by that factor as discussed in the main paper. Note that f_{sr} above can be used for scaling of emission of all complexes discussed in the main paper since emission of those is seen in PL always as a recombination of one electron and one hole, albeit Coulomb interacting slightly differently with each other.

SV. CONFIGURATION INTERACTION CODE WORKFLOW

1. Make a set of all possible SDs for a given multi-particle complex (X, X^+, X^-, XX, ...) and number of CI basis single-particle wavefunctions. Single-particle basis wavefunctions are represented by indices (index representation keeps RAM memory usage low).
2. Make all combinations of available SDs, keeping wavefunction index ordering of SDs (ordering reflects the different spatial positions of wavefunctions., i.e., r_1 or r_2) in such a way to form a following set: $\{\langle D_m^{\mathrm{M}}|, |D_n^{\mathrm{M}}\rangle\}$.
3. Discard all combinations in set $\{\langle D_m^{\mathrm{M}}|, |D_n^{\mathrm{M}}\rangle\}$ where wavefunction indices for third and higher positions (i.e. rs) in $\langle D_m^{\mathrm{M}}|$ and $|D_n^{\mathrm{M}}\rangle$ are different (that reflects single-particle wavefunction normalization condition). As a result we have $\{i, j, k, l\}$ wich are the only different indices between $|D_m^{\mathrm{M}}\rangle$ and $|D_n^{\mathrm{M}}\rangle$.
4. Find unique sets of $\{i, j, k, l\}$ occurring in the previous step (again spares RAM memory), compute Coulomb integrals for those unique sets and save the result in a set of unique Coulomb integrals.
5. Fill the upper (lower) triangular matrix of CI matrix by values from the preceding step and lower (upper) by complex conjugate of those values. Always check Hermiticity of the final CI matrix.
6. During the previous step compute also the oscillator strength overlaps as in Eq. (15) and store them in array.
7. Diagonalize CI matrix to obtain eigenvalues and eigenenergies.
8. Use the squares of absolute values of CI eigenenergies as weights of the single-particle oscillator strengths to obtain an emission rate of complex M. Multiply the result by the superradiance factor.

SVI. DEPENDENCE OF BINDING ENERGIES OF X^-, X^+, XX ON $\mathbf{k}\cdot\mathbf{p}$ SOLVER SETTINGS

In Fig. S1 the convergence of binding energies of X^-, X^+, and XX with respect to exciton are shown for different settings of the single-particle $\mathbf{k}\cdot\mathbf{p}$ solver. The varied settings of the single-particle solver included (i) the calculation of the elastic strain in the simulation structure and (ii) self-consistent solution of the Schrödinger and Poisson equations. The latter step effectively optimized the background electrostatic charge altered by the presence of the single-particle wavefunctions.

Note that while the CI calculations are converged for all studied multi-particle complexes, particularly in the case of XX the converged value is considerably different than the value from the measurements. Note further that from comparison of panels (a), (c) and (b), (d) in Fig. S1 it is clear that there is an influence of the self-consistent solution of the Poisson and Scrhödinger equations on the results of binding energies of X^-, X^+, and XX. That is expected because the aforementioned self-consistent cycle optimizes positions and spatial distributions of single-particle electron and hole states, leading effectively to the influence on the direct and exchange Coulomb intergrals computed within CI.[19]

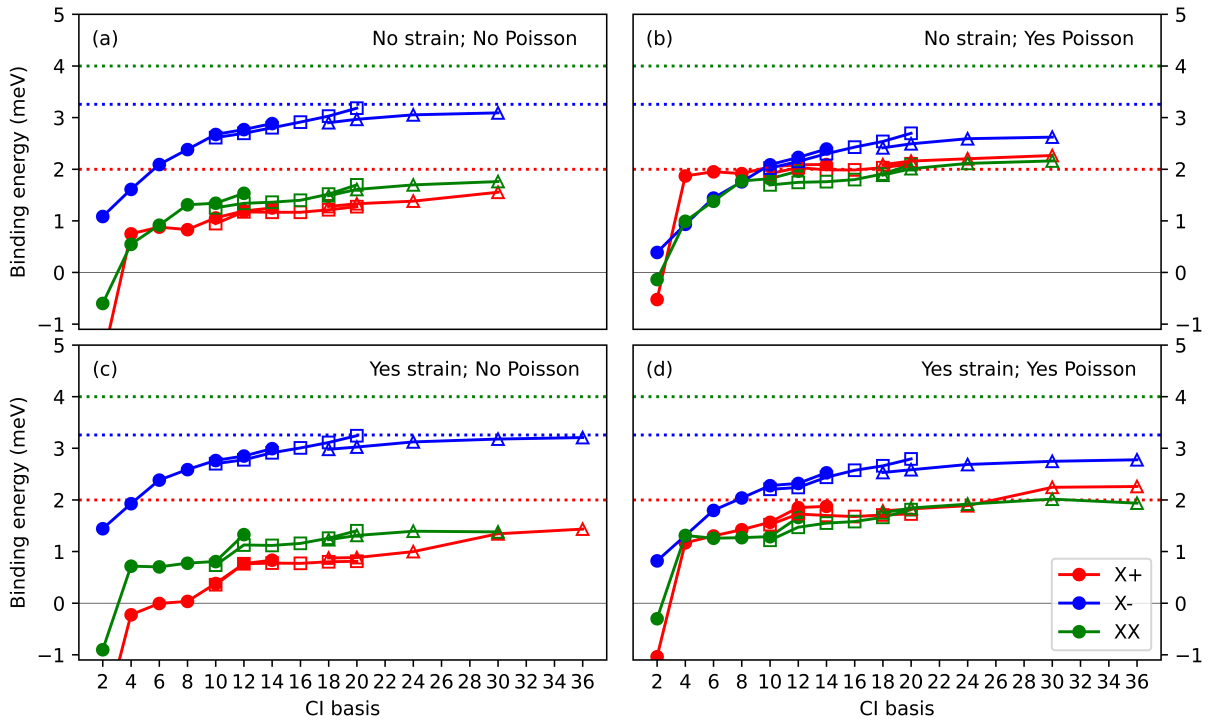

Figure S1. Binding energies of X^-, X^+, and XX with respect to exciton are shown as a function of CI basis size. The calculations are shown when (a) elastic strain in GaAs QD was not considered and the Poisson equation was not solved; in (b) the elastic strain was also not considered but the Schrödinger-Poisson cycle was performed; (c) when elastic strain in GaAs QD was considered but the Schrödinger-Poisson cycle was not computed; (d) when both elastic strain in QD was considered and the Schrödinger-Poisson cycle was performed. Note that panel (d) is the same as that in Fig. 2 (c) of the main paper. The red horizontal broken line denotes experimental binding energy of X^+ from Ref.[16], blue of X^- from Ref.[18], and green of XX from Ref.[11]. In all calculations in this figure the Coulomb exchange interaction was considered between all interacting quasiparticles.

SVII. DEPENDENCE OF BINDING ENERGIES OF X^-, X^+, XX ON ELECTRON-HOLE EXCHANGE

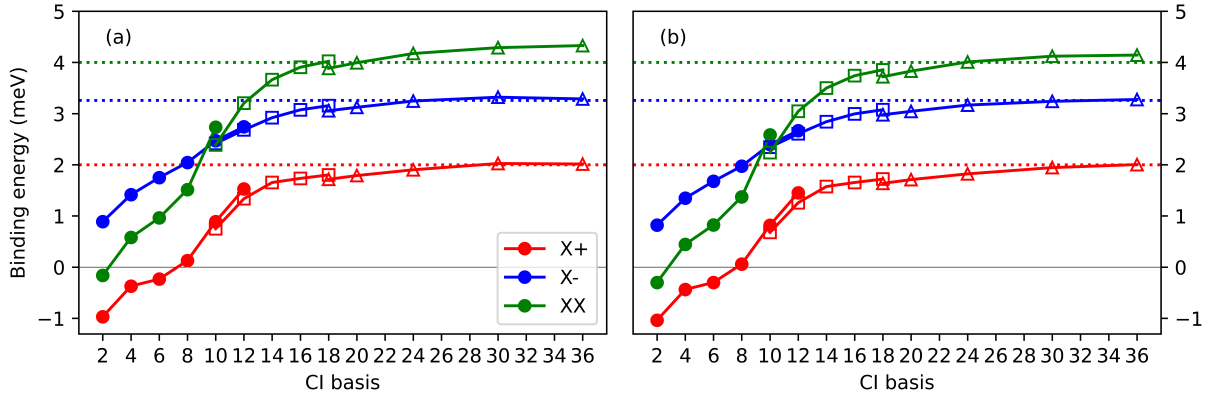

Figure S2. Binding energies of X^-, X^+, and XX with respect to exciton are shown as a function of CI basis size. The calculations are shown when (a) all Coulomb exchange was neglected and (b) when only electron-electron and hole-hole Coulomb exchange were neglected. Note that panel (c) is the same as that in Fig. 2 (d) of the main paper. The red horizontal broken line denotes experimental binding energy of X^+ from Ref.[16], blue of X^- from Ref.[18], and green of XX from Ref.[11].

In Fig. S2 the comparison between the calculation when all exchange interaction was neglected and that when only electron-electron and hole-hole exchange interaction was neglected is shown. Clearly, the difference between these calculations is small, confirming that the main reason for the large binding energy of the studied complexes is correlated direct Coulomb interaction.

We note that the binding energy of XX of ~ 4 meV in Fig. S2 (b) is close to the result of 3.4 meV[20] computed for a similar yet slightly different GaAs/AlGaAs QD by a phenomenological CI model that neglected the electron-electron and hole-hole exchange interaction and treated electron-hole exchange only phenomenologically, i.e. treating that as an input parameter taken from experiment.[20]

REFERENCES

[1] G. Bester, X. Wu, D. Vanderbilt, and A. Zunger, Physical Review Letters **96**, 187602 (2006).
[2] A. Beya-Wakata, P. Y. Prodhomme, and G. Bester, Physical Review B **84**, 195207 (2011).
[3] P. Klenovský, P. Steindl, J. Aberl, E. Zallo, R. Trotta, A. Rastelli, and T. Fromherz, Physical Review B **97**, 245314 (2018).
[4] P. Klenovský, P. Steindl, and D. Geffroy, Scientific Reports **7**, 45568 (2017).
[5] S. Birner, T. Zibold, T. Andlauer, T. Kubis, M. Sabathil, A. Trellakis, and P. Vogl, IEEE Transactions on Electron Devices **54**, 2137 (2007).
[6] T. Zibold, Ph.D. thesis, Technische Universität München, (2007).
[7] A. Schliwa, M. Winkelnkemper, and D. Bimberg, Physical Review B **79**, 075443 (2009).
[8] M. Zielinski, M. Korkusinski, and P. Hawrylak, Physical Review B **81**, 085301 (2010).
[9] P. Klenovský, D. Hemzal, P. Steindl, M. Zíková, V. Křápek, and J. Humlíček, Physical Review B **92**, 241302 (2015).
[10] P. Dirac, Proceedings of the Royal Society of London. Series A, Containing Papers of a Mathematical and Physical Character **114**, 243 (1927).
[11] S. F. C. da Silva, G. Undeutsch, B. Lehner, S. Manna, T. M. Krieger, M. Reindl, C. Schimpf, R. Trotta, and A. Rastelli, Applied Physics Letters **119**, 120502 (2021).
[12] S. Stobbe, P. T. Kristensen, J. E. Mortensen, J. M. Hvam, J. Mørk, and P. Lodahl, Physical Review B **86**, 085304 (2012).
[13] S. Stobbe, T. W. Schlereth, S. Höfling, A. Forchel, J. M. Hvam, and P. Lodahl, Physical Review B - Condensed Matter and Materials Physics **82** (2010).
[14] P. Tighineanu, R. S. Daveau, T. B. Lehmann, H. E. Beere, D. A. Ritchie, P. Lodahl, and S. Stobbe, Physical Review Letters **116** (2016).
[15] I. Vurgaftman, J. R. Meyer, and L. R. Ram-Mohan, Journal of Applied Physics **89**, 5815 (2001).
[16] X. Yuan, S. F. C. D. Silva, D. Csontosová, H. Huang, C. Schimpf, M. Reindl, J. Lu, Z. Ni, A. Rastelli, and P. Klenovský, Physical Review B **107**, 235412 (2023).
[17] D. Csontosová and P. Klenovský, Physical Review B **102**, 125412 (2020).
[18] D. Huber, B. U. Lehner, D. Csontosová, M. Reindl, S. Schuler, S. F. Covre da Silva, P. Klenovský, and A. Rastelli, Physical Review B **100**, 235425 (2019).
[19] G. Hönig, G. Callsen, A. Schliwa, S. Kalinowski, C. Kindel, S. Kako, Y. Arakawa, D. Bimberg, and A. Hoffmann, Nature Communications **5**, 5721 (2014).
[20] B. U. Lehner, T. Seidelmann, G. Undeutsch, C. Schimpf, S. Manna, M. Gawełczyk, S. F. C. da Silva, X. Yuan, S. Stroj, D. E. Reiter, V. M. Axt, and A. Rastelli, Nano Letters **23**, 1409 (2023).